Contents lists available at ScienceDirect

Bioactive Materials

journal homepage: www.keaipublishing.com/en/journals/bioactive-materials

Engineered human spinal cord-like tissues with dorsal and ventral neuronal progenitors for spinal cord injury repair in rats and monkeys

Bai Xu [a,b,1], Dingyang Liu [c,d,1], Weiyuan Liu [a,1], Ge Long [e], Wenbin Liu [a], Yayu Wu [a], Xinghui He [c,d], Yeyu Shen [d,f], Peipei Jiang [g], Man Yin [a], Yongheng Fan [a], He Shen [h], Liyang Shi [i], Qi Zhang [a], Weiwei Xue [a], Chen Jin [a], Zhenni Chen [a], Bing Chen [a], Jiayin Li [a], Yali Hu [g], Xing Li [d,**], Zhifeng Xiao [a,***], Yannan Zhao [a,****], Jianwu Dai [a,h,*]

[a] State Key Laboratory of Molecular Developmental Biology, Institute of Genetics and Developmental Biology, Chinese Academy of Sciences, Beijing, 100101, China
[b] Wuxi School of Medicine, Jiangnan University, Wuxi, 214122, China
[c] Department of Neurosurgery, Xiangya Hospital of Central South University, Changsha, 410008, China
[d] College of Life Science, Central South University, Changsha, 410078, China
[e] Department of Anesthesia, The Third Xiangya Hospital of Central South University, Changsha, 410013, China
[f] Department of Spine Surgery, Xiangya Hospital of Central South University, Changsha, 410008, China
[g] Department of Obstetrics and Gynecology, The Affiliated Drum Tower Hospital of Nanjing University Medical School, Nanjing, 210008, China
[h] Division of Nanobiomedicine, Suzhou Institute of Nano-Tech and Nano-Bionics, Chinese Academy of Sciences, Suzhou, 215123, China
[i] College of Biology, Hunan University, Changsha, 410012, China

ARTICLE INFO

ABSTRACT

Transplanting human neural progenitor cells is a promising method of replenishing the lost neurons after spinal cord injury (SCI), but differentiating neural progenitor cells into the diverse types of mature functional spinal cord neurons *in vivo* is challenging. In this study, engineered human embryonic spinal cord-like tissues with dorsal and ventral neuronal characters (DV-SC) were generated by inducing human neural progenitor cells (hscNPCs) to differentiate into various types of dorsal and ventral neuronal cells on collagen scaffold *in vitro*. Transplantation of DV-SC into complete SCI models in rats and monkeys showed better therapeutic effects than undifferentiated hscNPCs, including pronounced cell survival and maturation. DV-SC formed a targeted connection with the host's ascending and descending axons, partially restored interrupted neural circuits, and improved motor evoked potentials and the hindlimb function of animals with SCI. This suggests that the transplantation of pre-differentiated hscNPCs with spinal cord dorsal and ventral neuronal characteristics could be a promising strategy for SCI repair.

1. Introduction

SCI results in permanent motor and sensory function deficits below the injured segment. It has been estimated that three million people live with traumatic SCI worldwide, with approximately 180,000 new cases announced each year [1]. There is currently no efficient clinical therapy for SCI, until recently [2]. Since neural progenitor cells (NPCs) can multi-directionally differentiate into neurons, astrocytes, and oligo-dendrocytes, NPC transplantation is considered a promising method for replenishing lost cells in the lesion site after SCI [3–10].

NPCs transplantation currently faces several challenges. First, grafted NPCs are inclined to differentiate into astrocytes in the injured spinal

cord due to an inhibitory microenvironment after SCI [11–18]. Second, the spinal cord contains more than 20 distinct neuron subpopulations that are responsible for sensory and locomotive behavior. During embryonic mouse spinal cord development, 12 neuronal restricted progenitor domains are formed along the dorsoventral axis of the neural tube. These neuronal restricted progenitors can result in cardinal classes of dorsal interneurons (INs), cardinal classes of ventral INs, and motor neurons (MNs) [19]. The neuronal population of the spinal cord is largely conserved between rodents and human beings [20]. While some literature has reported that grafted NPCs can differentiate into specific neurons [19,21], regenerating various lost neurons after SCI is difficult. Third, the long differentiation and maturation period of human NPCs is insufficient for producing mature neurons during the short therapeutic window after SCI. Human spinal cord NPCs (hscNPCs) required a longer time to develop into mature neurons, typically at least several months [20,22–26]. We hypothesize that the pre-differentiation of hscNPCs into dorsal or ventral neuronal cells before transplantation could be important for stem cell-based SCI repair.

In this study, we isolated and cultured early embryonic hscNPCs on a collagen scaffold. We induced them to differentiate into several types of dorsal and ventral neuronal progenitors with different cocktails *in vitro* to generate engineered dorsal and ventral spinal cord-like tissues (DV-SC). We then transplanted DV-SC into rats with complete transection SCI to examine the survival and maturation of pre-differentiated dorsal and ventral neuronal progenitors and electrophysiological and motor function recovery. Considering monkey models are important for human trials because they share a similar body size, neuroanatomy, complexity of neurological functions, and immunology [27], we also grafted DV-SC into rhesus monkeys with complete transection SCI to assess the therapeutic outcomes. These data demonstrate that the transplantation of pre-differentiated hscNPCs with spinal cord dorsal and ventral neuronal characters could be a promising strategy for SCI repair.

2. Material and methods

2.1. Ethics

Rats were supplied and housed at the experimental animal center at the Institute of Genetics and Developmental Biology, Chinese Academy of Sciences (Bejing, China), and all surgeries were performed there. Rhesus monkeys were supplied and housed at the experimental animal center in Hunan Puruima Medicine Research Center (Hunan, China), and all surgeries were performed there. All experimental and surgical procedures were performed in accordance with the Chinese Ministry of Public Health Guide and were approved by the Institutional Animal Care and Use Committee of Hunan Puruima Medicine Research Center.

The use of human embryo tissues for cell culturing was approved by the Reproductive Study Ethics Committee of Nanjing Drum Tower Hospital and Nanjing Medical University (2018-223-01). Informed consent was provided by the donors. The aborted embryo tissues were acquired from legally terminated pregnancies [20].

2.2. HscNPCs culture

Gestational 7-week-old human embryo tissue was obtained from Nanjing Drum Tower Hospital after normal termination in accordance with nationally approved ethical and legal guidelines. HscNPCs culture was carried out as previously reported [28–30]. Primary NPCs were obtained from 2-cm-long human spinal cord tissues at gestational 7 weeks. The single-cell suspension of spinal cord was prepared at 37 °C with accutase (Sigma-Aldrich, USA) for 5 min. Next, an appropriate volume of Dulbecco's modified Eagle's medium (DMEM)/F-12 medium was added to end the digestion, and the suspension was centrifuged at 500 g for 5 min. Cells were cultured in 10-cm wide petri dishes (Corning, USA), pre-coated with 125 μg laminin (BioLamina, Sweden) in the proliferation medium (2:1 mixture of DMEM and DMEM/F12, Gibco,

USA) containing 1% non-essential amino acid (Gibco, USA), 1% sodium pyruvate (Gibco, USA), 1% penicillin-streptomycin (Gibco, USA), 15 mM HEPEs (Sigma-Aldrich, USA), 2% B27 (Gibco, USA), 100 mg/L human plasma apo-transferrin (Millipore, USA), 25 mg/L recombinant human insulin (Yeasen, Shanghai, China), 15 g/L glucose (Sigma-Aldrich, USA), 20 nM progesterone (Sigma-Aldrich, USA), 100 μM putrescine (Sigma-Aldrich, USA), 30 nM sodium selenite (Sigma-Aldrich, USA), 40 ng/mL epidermal growth factor (EGF, Peprotech, USA), 40 ng/mL basic fibroblast growth factor (bFGF, Peprotech, USA), 20 ng/mL leukemia inhibitory factor (LIF, Peprotech, USA), 10 ng/mL neurotrophins-3 (Peprotech, USA), and 1.83 μg/L heparin (Sigma-Aldrich, USA).

The medium was changed for each sample every other day. HscNPCs reached the primary culture stage at 15 days, and then were passaged approximately every 7 days, when they grew to 80% confluence. During the process of passaging, HscNPCs were digested with accutase, then replated onto new 10 cm petri dishes precoated with laminin at a density of 1×10^6 cells per dish. HscNPCs could be passaged for at least ten generations and cells at the sixth passage were used for following experiments in this study.

To track the grafted hscNPCs *in vivo*, the cells were infected with a lentivirus expressing green fluorescent protein (GFP; Miga Technology Co., Ltd, China). Briefly, when hscNPCs reached about 50% confluence, the culture medium was changed to fresh proliferation growth medium containing the lentivirus (10^8 TU/mL, 50 μL GFP lentivirus per 10^6 hscNPCs), polybrene (5 mg/mL, Miga Technology Co., Ltd, China) was used to increase viral attachment. 8 h later, the proliferation medium was changed again to remove the lentivirus. After incubating at 37 °C for 72 h, these cells were seeded on the collagen scaffolds.

2.3. Scaffold preparation and characterization

The collagen scaffold was produced as previously reported [15]. Briefly, the depilated bovine skin was immersed in 0.5 M acetic acid solution at 4 °C. Next, samples were mixed in a blender for 15 min and neutralized with 4 M NaOH to obtain a uniform collagen solution. After dialysis and lyophilization, the collagen scaffold was acquired. To generate an aligned porous structure, the collagen scaffolds were cut into $0.2 \times 0.5 \times 0.5$ cm blocks and infiltrated in 40 mL MES (pH 6.5) containing 0.6 mg/mL N-hydroxysuccinimide and 1 mg/mL 1-ethyl-3-(3-dimethylaminopropyl) carbodiimide. The pellets were then washed. A mechanical-testing machine (Shimadzu AGS-X, Japan) was used to examine the mechanical properties of the collagen scaffold. Stretching strain data at various stretching stresses were recorded (n = 4 samples). Collagenase I was used to degrade the collagen scaffolds. Specifically, 0.16 mg/ml (i.e. 40 U/mL) of collagenase I was dissolved in Tris-EDTA-SDS-CaCl$_2$ TESCA buffer and then the collagen scaffolds were digested at 37 °C. For scanning electron microscope (SEM), collagen scaffold or collagen scaffold loaded with cells were washed three times with PBS, then fixed in 2.5% glutaraldehyde for approximately 90 min, dehydrated with a range of graded ethanol, and freeze-dried for 2 d. Finally, the dried samples were coated with gold and examined under SEM.

2.4. Generation of a DV-SC

We induced dorsal or ventral differentiation of hscNPCs by simulating the development process of the embryonic spinal cord [19, 31–38]. To make a DV-SC, we seeded hscNPCs onto semicircular piece of collagen scaffold and pre-differentiated into dorsal or ventral hscNPCs. To promote the cell adhesion on the collagen scaffold, we prepared 10 μg/mL laminin with PBS, and the collagen scaffold were immersed into the laminin solution at 37 °C for 2 h. Then the collagen scaffolds were rinsed in PBS once and the excess PBS was removed by a sterilized filter paper. HscNPCs were digested and the density of cell suspension was adjusted to 5×10^5 cells/5 μL in the proliferation medium, and then cells

were carefully added onto each half of collagen scaffold. For rat transplantation, the total seeding number of hscNPCs was 10^6, and for rhesus monkey transplantation, the total cell seeding number was 10^7. After that, collagen scaffolds loaded with hscNPCs were cultured at 37 °C for 2 h. HscNPCs began to extend and adhere to the porous collagen scaffolds during this phase. Then sufficient differentiation medium was added into the cell culture plate for subsequent induction. HscNPCs loaded on the collagen scaffolds were differentiated in the dorsal or ventral differentiation medium respectively for 30 d *in vitro*.

Compared with the proliferation medium, the basal differentiation medium had no growth factors, such as EGF, bFGF, or LIF. However, we added 10 ng/mL brain-derived neurotrophic factor (BDNF, Peprotech, USA) and 20 ng/mL glial cell line-derived neurotrophic factor (GDNF, Peprotech, USA) to promote the survival and maturation of the neurons. For dorsal differentiation, we added an additional 15 ng/mL of bone morphogenetic protein 4 (BMP4), which belonged to the transforming growth factor-β family of proteins in the differentiation medium. The ventral differentiation medium was supplemented with some small molecules and factors, including 100 nM SAG (a small molecule that acts as a smoothened agonist of SHH signaling), 0.2 μM LDN-193189 (a small molecule to inhibit BMP signaling) [32,39–43], 100 nM retinoic acid, 10 ng/mL ciliary neurotrophic factor, 10 ng/mL insulin-like growth factor-1, and 1 μM adenosine cyclophosphate.

2.5. Immunocytochemistry

After 30 d culture, hscNPCs seeded on collagen scaffolds were fixed in 4% paraformaldehyde (PFA) for 15 min at room temperature (RT). After being washed three times with phosphate buffer saline (PBS), fixed samples were permeabilized with 0.2% Triton X-100 with 5% normal donkey serum in fetal bovine serum for 1 h. Primary antibodies diluted in the blocking solution were applied overnight. The primary antibodies used for immunolabeling are recorded in Supplementary Table 1. For quantification of dorsal and ventral neuronal markers in DV-SC, the differentiation assay was performed for three times. Images were taken from randomly selected three fields in each subject by using a confocal microscopy (Zeiss, Observer.Z1). A total number of 9 images were used for quantification for each subject. DAPI positive signal intensity was thresholded and counted automatically using ImageJ. BRN3A$^+$, TLX3$^+$, LMX1B$^+$, FOXP2$^+$, LHX1$^+$, HB9$^+$, ISL1$^+$, and OLIG2$^+$ immunostained cells were counted manually. Then percentage of dorsal and ventral INs, MNs or motor neuron progenitors (MNPs) were calculated.

2.6. Quantitative real-time polymerase chain reaction (Q-PCR) analysis

Total RNA was extracted using an Ultrapure RNA Kit (Cowin Biosciences, Jiangsu, China). For cDNA synthesis, the reverse-transcription reaction was performed using a reverse transcription kit (Hifair II 1st Strand cDNA Synthesis Super Mix for qPCR, YEASEN 11123ES60). Q-PCR was performed using SYBR Green Master Mix (Hifair qPCR SYBR Green Master Mix, YEASEN 11201ES08) to detect mRNA abundance. The primers were shown in Supplementary Table 2.

2.7. Whole-cell patch clamp

Differentiated dorsal or ventral hscNPCs were harvested and were maintained in a 24-well plate filled with 500 μL of differentiation medium in an incubator (5% CO2, 37 °C). After a recovery period of approximately 1 h, an individual cell cluster was moved to a recording chamber and continuously superfused with oxygenated artificial cerebrospinal fluid (in mM: 126 NaCl, 331 KCl, 26 NaHCO3, 1.2 NaH2PO4, 2.4 CaCl2, 1.3 MgCl2 and 10 D-glucose) at a rate of 3–5 mL per minute at 30 ± 1 °C. An inverted microscope (IX73, Olympus, Japan) equipped with epifluorescence and infrared-differential interference contrast (DIC) illumination, and a camera (Andor), air immersion lens (40X), and air immersion lens (4X) were used to visualize the cells and operate

electrodes. Patch pipettes had a 5–7 MΩ resistance when full of intracellular solution (in mM: 10 HEPES, 130 potassium gluconate, 16 KCl, 2 MgCl2, 4 Na2-ATP, 0.4 Na3-GTP, 0.2171 EGTA and 0.5% neurobiotin, pH = 7.25, adjusted with KOH). Evoked action potentials were recorded in current-clamp mode using a set of injected currents from −100 pA to 280 pA in increments of 20 pA. Na–K currents were recorded in voltage-clamp mode with a basal holding potential of −70 mV followed by stimulating pulses from −80 mV to 60 mV with a step size of 10 mV. The membrane potential was held at −70 mV when spontaneous excitatory postsynaptic currents were recorded. Stimulus delivery and data acquisition were conducted with a multiclamp 700B amplifier and a Digidata 1440 A (Molecular Devices, USA), which were controlled by Clampex.

2.8. Surgery procedures for rats

A Sprague Dawley rat T8-9 spinal cord complete transection model was made with a microscissor. Rats used in the experiment were 6–8 week-old females weighing 200–220 g. The surgery procedure was slightly modified according to the previous reports [44,45]. All surgeries were performed under intraperitoneal anesthesia with a 10% chloral hydrate solution (500 mg/kg), after which a 2–3 cm midline incision was made to reveal the T8-11 vertebrae. After removing the laminae, the spinal cord was exposed, and a 3–4 mm long segment of the spinal cord was excised in T8-9. Bleeding was stopped using a gelatin sponge filled up in the transection site. Immediately following surgery, collagen scaffolds, collagen scaffolds loaded with undifferentiated hscNPCs, or pre-differentiated dorsal and ventral hscNPCs were transplanted into the gap. Rats were randomly assigned into three experimental groups, with 20 rats per group. Group one received only transplantation of collagen scaffolds (scaffold group), group two received transplantation of collagen scaffolds loaded with 10^6 undifferentiated hscNPCs (scaffold + NPCs group), and group three received transplantation of collagen scaffolds loaded with 10^6 pre-differentiated dorsal and ventral hscNPCs (scaffold + DV-SC group). There were 14, 15, 14, and 15 rats that survived in each group, respectively. Following treatments, the skin and musculature were closed with sutures, and each group of rats was returned to their respective cages to recover. In addition, in groups that received cell implantation, cyclosporin A (10 mg/kg/rat/d, MedChemExpress, MCE, USA) was injected intraperitoneally 3 d before surgery and continued daily in all rats until they were euthanized.

2.9. Surgery procedures for rhesus monkeys

A total of 19 adult female rhesus monkeys (*Macaca mulatta*), aged 3–4 years old and weighing 4.1–5.8 kg were used in this study. All rhesus monkeys were placed into individual cages at a temperature of approximately 16–22 °C, and 40–70% humidity. Before surgeries, rhesus monkeys were housed in animal quarters for at least 3 weeks. The rhesus monkeys were randomly divided into three groups: 1) four in the control group without any treatment, 2) six in the collagen scaffolds + 10^7 undifferentiated hscNPCs graft group (scaffold + NPCs group), and 3) nine in the collagen scaffolds + 10^7 pre-differentiated dorsal and ventral hscNPCs graft group (scaffold + DV-SC group). The 9 monkeys transplanted with scaffold + DV-SC were sacrificed at the following different time point, including: 1) 1 monkey sacrificed at 7 days post injury (dpi); 2) 1 monkey sacrificed at 20 dpi; 3) 3 monkeys sacrificed at 2 months post injury (mpi); 4) 1 monkey sacrificed at 4 mpi; 5) 3 monkeys sacrificed at 6 mpi.

Rhesus monkeys were anesthetized with tiletamine-zolazepam (Zoletil 50; Virbac S.A., Carros, France) at a dose of 5 mg/kg, and administered an intramuscular injection of 0.1 mg/kg atropine sulfate after 8–10 h of food and water deprivation. After being anesthetized, tracheal intubation was conducted, and mechanical ventilation was applied. Anesthesia was maintained by fentanyl (7–10 μg/kg/h intravenously, Hospira Inc., Lake Forest, IL) and propofol (2.5 mg/kg/rhesus

monkey, intravenously, ASTRAZENECA PLC, UK). An intravenous infusion of physiological saline was administered to preserve blood volume. The respiratory rate, heart rate, and blood oxygen saturation were monitored during the surgery. Under aseptic conditions, a 4–6 cm longitudinal incision was made at T8-10. The erector spine muscle was dissected away from the spinous process. A 5–6 mm long segment of the spinal cord in T8-9 was excised using previously reported methods [46, 47]. After thorough hemostasis with gel foam, a 7–8 mm diameter and 6 mm long collagen scaffold loaded with 10^7 undifferentiated hscNPCs or 10^7 pre-differentiated dorsal and ventral hscNPCs was implanted to fill the transected cavity. The control group underwent T8-9 complete spinal cord transection without any additional treatment. Finally, dura, paraspinal muscles, and skin were closed in layers with sutures. In groups that received cell implantation, tacrolimus (1 mg/kg/rhesus monkey/d, Astellas Ireland Co., Ltd, Ireland), mycophenolate mofetil (100 mg/kg/rhesus monkey/d, Coche Pharmaceuticals Ltd, Switzerland), and prednisone acetate (1 mg/kg/rhesus monkey/d, Xianju Pharmaceutical Co., Ltd, Zhejiang, China) were injected intraperitoneally 3 d before surgery and continued daily in all rhesus monkeys until sacrificed. Since a complete transection would result in paraplegia and loss of bowel and bladder function, we hired specialized staff to empty the monkey bladders 2–3 times a day.

2.10. Behavioral assessments

Weekly behavioral evaluations were performed on the rats by two observers blinded to the post-injury treatments, using the Basso, Beattie & Bresnahan (BBB) locomotor rating scale to check walking ability and motion amplitude, fineness, and coordination of the three hind limb joints.

Analysis of the rhesus monkeys' movement was recorded as previously described [48,49]. Videos were recorded and evaluated by two individual, blinded investigators. Finally, 4 videos were shown, including Supplementary Video S2 showing DV-SC at 6 mpi, Supplementary Video S3 showing DV-SC at 3 mpi, Supplementary Video S4 showing control at 6 mpi, and Supplementary Video S5 showing scaffold + NPCs at 6 mpi.

Supplementary data related to this article can be found at https://doi.org/10.1016/j.bioactmat.2023.03.015.

2.11. Electrophysiology assessment

The cortical motor evoked potentials (CMEPs) of rats were evaluated at 8 weeks post-injury (wpi) after SCI using Keypoint 9033A07 (Alpine bioMed ApS, Denmark). Rats were anesthetized with chloral hydrate solution (500 mg/kg) and placed in a prone position for the testing operation. For CMEPs, the stimulus electrode was placed into the subcutaneous tissue 1 cm behind the intersection of the cranial midline and eyebrow, and the other electrode was placed into the contralateral subcutaneous tissue. The recording electrode was inserted into the muscle of one hindleg. The grounding electrode was placed subcutaneously near the L1 spinal segment. Multiple pulse stimulation was used to produce a CMEPs wave with the following parameters: 45 mA, 0.1 ms, and 2 Hz. Each test was repeated five times to ensure waveform stability.

Spinal cord motor evoked potentials (SCMEPs) of rhesus monkeys were detected as described before [46,50]. The stimulating electrodes were inserted into the host rostral section of the lesion site, and the recording electrodes were inserted into the host caudal section of the lesion site. The reference electrodes were inserted into the tail.

2.12. Immunohistochemistry

The animals were deeply anesthetized with 10% chloral hydrate (500 mg/kg) and transcardially perfused with 0.9% NaCl physiological saline solution, followed by treatment with 4% PFA. Immediately after perfusion, spinal cords were dissected, post-fixed overnight at 4 °C, and separately transferred to 20% sucrose and 30% sucrose overnight at 4 °C. Horizontal sections of spinal cords containing the transection/graft site (approximately 2 cm long) were sectioned on a cryostat set at 18–20 μm thickness. Cryosections were permeabilized with 0.2% Triton X-100 with 5% normal donkey serum in fetal bovine serum for 1 h at RT, after which the blocking buffer was removed and replaced with primary antibodies. All primary antibodies are listed in Supplementary Table 2.

For quantification of surviving cells after surgery, the number of GFP-labeled grafted cells was quantified from 56 continuous sagittal slices (18 μm-thick per slice) in the lesion site from three rats or 150 continuous sagittal slices (20 μm-thick per slice) in the lesion site from three monkeys at each time point. Total number of graft cells per subject was estimated by quantifying for GFP in every seventh section in rats and in every fifteenth section in monkeys, then multiplied by 7 or 15, respectively. GFP positive signal intensity was thresholded and counted automatically using ImageJ.

To quantify the cell type of GFP-positive cells, neuronal class III β-tubulin (TUJ1) and NeuN antibodies were used for distinguishing neurons. 5-hydroxytryptamine (5-HT), peptidergic C-fibers expressing calcitonin gene-related peptide (CGRP), SYP and PSD95 were detected in the lesion region of three rats and three monkeys at each time point. Images were taken from three randomly selected fields in the lesion site and boundary site between normal tissue and injury area in each slice on a confocal microscope (Leica). A total number of 6 images were used for quantification for each subject. GFP$^+$/TUJ1$^+$ or GFP$^+$/NeuN$^+$ double-immunostained neurons and GFP$^+$ cells were counted manually, and calculated for percentage of transplanted neurons in GFP$^+$ graft cells.

To quantify neuronal subtypes in DV-SC grafts, neuronal subtype transcription factors (BRN3A, TLX3, LMX1B, HB9, ISL1, FOXP2, and SIM1) and GFP co-labeled sections from three rats and three monkeys were used. Images were taken from three randomly selected fields in the lesion site and boundary site between normal tissue and injury area in each slice on a confocal microscope (Zeiss, Observer.Z1). A total number of 6 images were used for quantification for each subject. GFP$^+$/BRN3A$^+$, GFP$^+$/TLX3$^+$, GFP$^+$/LMX1B$^+$, GFP$^+$/HB9$^+$, GFP$^+$/ISL1$^+$, GFP$^+$/FOXP2$^+$, and GFP$^+$/SIM1$^+$ double-immunostained neurons and GFP$^+$ cells were counted manually, and calculated for percentage of dorsal and ventral neurons in DV-SC grafts.

2.13. Statistical analysis

All experiments were repeated at least three times and statistical analysis were performed with GraphPad Prism 7. Randomization of animal studies was used in the data analysis. All data were presented as means ± standard deviation. Data points that were above (mean + 2 standard deviation) and points below (mean - 2 standard deviations) were eliminated. Two-group comparisons were tested by a two-tailed unpaired Student's *t*-test in which the data were subjected to normal distribution. One-way repeated-measures ANOVA was conducted to examine the differences between multiple groups in which the data were subject to normal distribution. $P < 0.05$ was considered statistically significant. * represents P-value <0.05, ** represents P-value <0.01, *** represents P-value <0.001.

3. Results

3.1. Phenotypic characterization of HscNPCs

HscNPCs were isolated from gestational 7-week-old embryonic spinal cord tissues. We first identified hscNPCs characteristics, which could be continuously passaged for at least ten generations *in vitro*. Immunofluorescence staining and quantitative analysis revealed that 16.3% ± 4.2% of them expressed the proliferative marker Ki67 (Fig. 1A and B). Approximately 95.2% ± 10.3% of cells expressed Nestin, and 91.5% ± 5.4% expressed SOX2, both of which are NPCs markers, and 89.2% ± 8.1% expressed TUJ1, which is a marker for neural progenitors or early
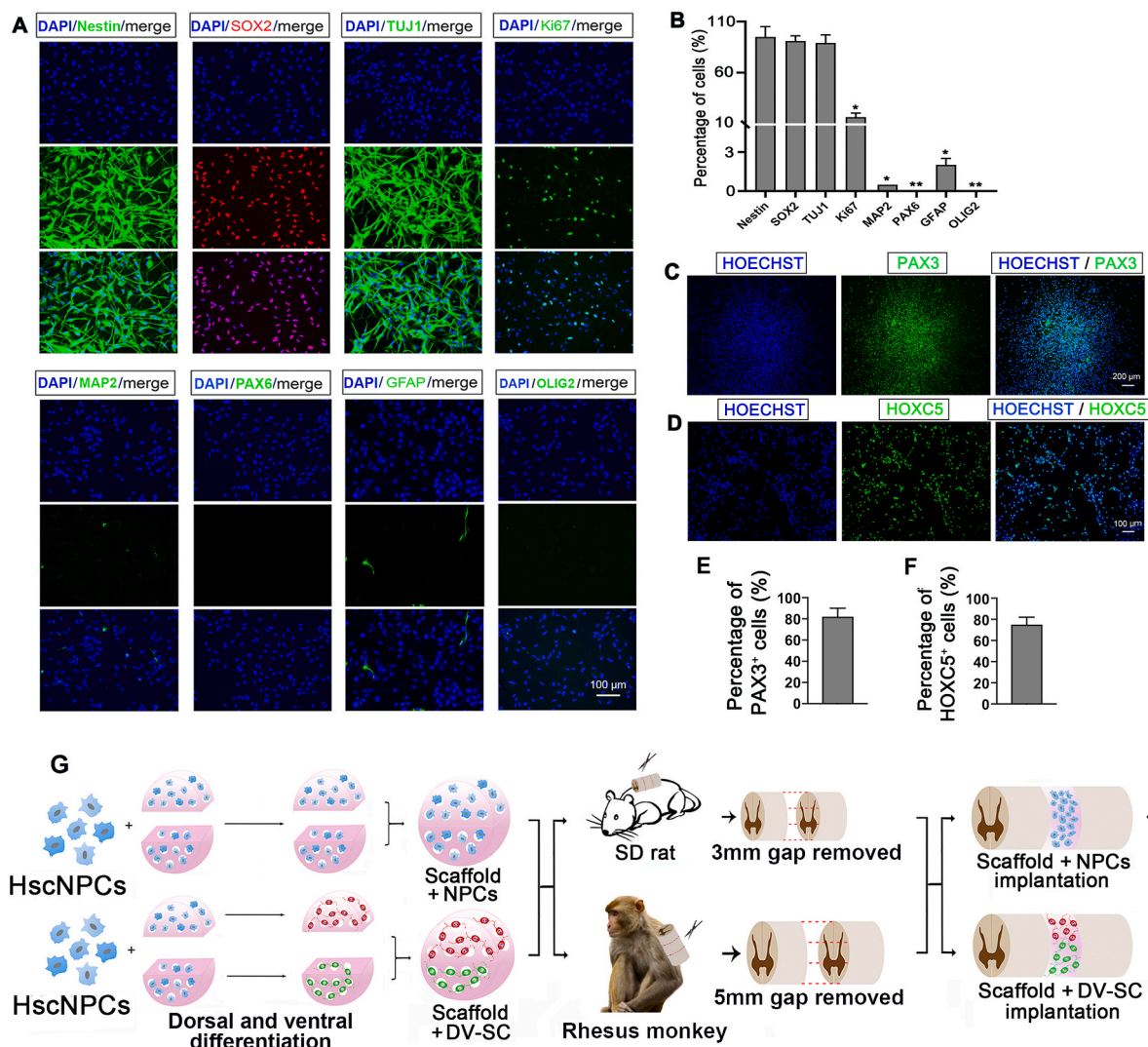
Fig. 1. Characterization of hscNPCs. (**A**) Immunofluorescence staining with various developmental markers. Scale bar = 100 μm. (**B**) Quantification of the percentage of various markers in (**A**). *p < 0.05, **p < 0.01, both compared with Nestin. Immunofluorescence staining with (**C**) spinal cord dorsal progenitor marker PAX3. Scale bar = 200 μm. and (**D**) cervical marker HOXC5. Scale bar = 100 μm. Quantification of (**E**) percentage of PAX3$^+$ cells. and (**F**) percentage of HOXC5$^+$ cells. (**G**) Schematic diagram of DV-SC transplantation in SCI rats and rhesus monkeys.

neurons (Fig. 1A and B). However, MAP2 (mature neuron marker), GFAP (astrocyte marker), and OLIG2 (oligodendrocyte marker) were rarely expressed (Fig. 1A and B). Additionally, we noticed that 70.5% ± 7.7% of these cells expressed the cervical spinal cord gene marker HOXC5 [51] (Fig. 1D and F) and about 85.2% ± 10.1% of the cells expressed PAX3 (Fig. 1C and E), which is a marker of spinal cord neural progenitors [19]. In order to further characterize the hscNPCs, we performed Q-PCR analysis (Supplementary Fig. 1A and Supplementary Fig. 1B) and immunostaining using dorsal and ventral regional marker antibodies, such as BRN3A, TLX3, FOXP2, and LHX3 (Supplementary Fig. 1D) [19]. Schematic diagram of expression of spinal cord neuronal progenitors markers was shown in Supplementary Fig. 1C. Microscopic photos of hscNPCs and immunofluorescence staining of GFP-transfected hscNPCs were shown in Supplementary Fig. 1E and Supplementary Fig. 1F. Together with these data, we propose hscNPCs are negative for ventral or dorsal regional markers of spinal cord before dorsal or ventral induction. These results show that these cells primarily consist of immature spinal cord-derived neural progenitors. After characterizing hscNPCs, we seeded hscNPCs on the collagen scaffold for dorsal or ventral induction before transplantation, and the schematic diagram of transplantation in spinal cord injured rats and rhesus monkeys were shown in Fig. 1G.

3.2. Construction of engineered human spinal cord-like tissues with dorsal and ventral neuronal progenitors

To construct pre-differentiated spinal cord-like tissues from hscNPCs, porous collagen scaffolds with similar cylindrical structure to spinal cords were fabricated in this study. The SEM images displayed that there were many tiny pores and longitudinally ordered structures inside the scaffold (Fig. 2A and B). *In vitro*, the collagen scaffolds could be totally degraded in collagenase I. The complete degradation time of the collagen scaffolds in 40 U/mL of collagenase I at 37 °C was within 120 h. The degradation rate of the collagen scaffold in collagenase was about 0.686 ± 0.132 μg/h·IU. The elasticity modulus of the collagen scaffold was about 25.25 ± 1.951 kPa. HscNPCs cultured on a collagen scaffold showed that cells could extend long axons on the sacffold (Fig. 2C). Cell viability was measured by AO/PI staining. 10^6 hscNPCs cultured on a collagen scaffold were all alive after cultured for 2 weeks (Fig. 2D).

To obtain mature spinal cord dorsal or ventral INs, the half-cylinder scaffolds with hscNPCs were incubated with different cocktails for dorsal or ventral induction, respectively. The engineered human embryonic spinal cord-like tissues with dorsal and ventral neuronal characters were generated with this method (Fig. 2E and F). According to the morphogens during spinal cord development, BMP4 was added to the
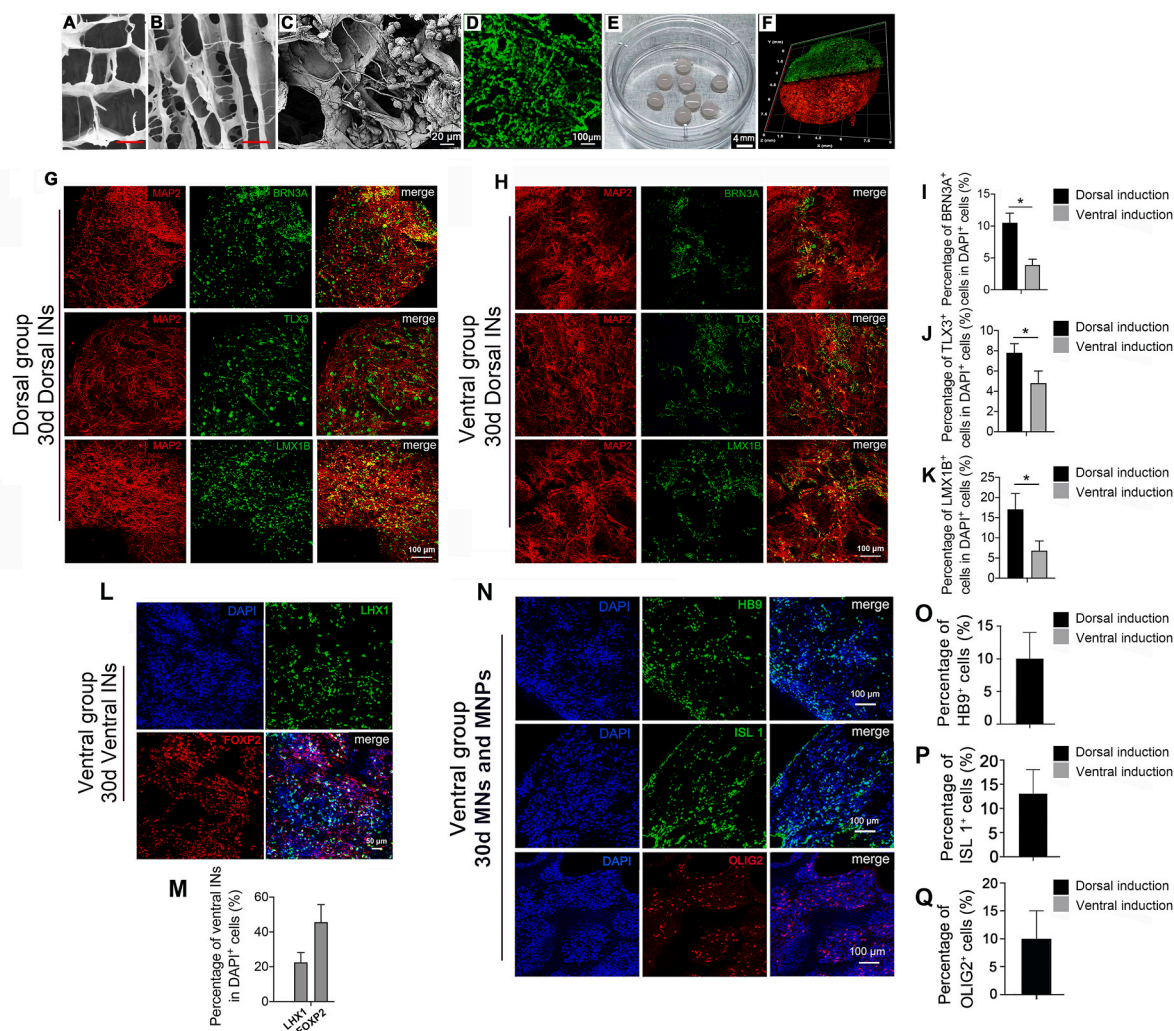
Fig. 2. Construction of engineered human spinal cord-like tissues with dorsal and ventral neuronal progenitors. SEM images showing (**A**) cross-sectional morphology of the collagen scaffold. Scale bar = 30 μm, and (**B**) longitudinal sectional morphology of the collagen scaffold. Scale bar = 60 μm, and (**C**) hscNPCs cultured on the collagen scaffold for 2 w. Scale bar = 20 μm. (**D**) Confocal image of AO/PI staining of hscNPCs cultured on collagen scaffold for 2 w. Scale bar = 100 μm. (**E**) Macroscopic image of collagen scaffolds loaded with hscNPCs. Scale bar = 4 mm. (**F**) A schematic diagram of the assembling pattern of pre-differentiated dorsal and ventral hscNPCs *in vitro*. HscNPCs were seeded onto each piece of collagen scaffold and separately pre-differentiated into dorsal or ventral hscNPCs. Cells on the dorsal or ventral piece of collagen scaffold were individually labeled with Dil at a dilution ratio of 1:1000 and PKH67 at a dilution ratio of 1:500. The diameter of collagen scaffold used for rhesus monkey SCI transplantation was approximately 6 mm. Immunofluorescence staining of spinal cord dorsal INs markers of hscNPCs cultured in (**G**) dorsal medium or (**H**) ventral medium for 30 d *in vitro*, scale bar = 100 μm. Quantification of percentage of (**I**) BRN3A⁺ cells, (**J**) TLX3⁺ cells, (**K**) LMX1B⁺ cells in DAPI⁺ cells. *p < 0.05. Immunofluorescence staining of spinal cord (**L**) ventral INs markers, scale bar = 50 μm, and (**N**) MNs and MNPs markers of hscNPCs cultured in ventral medium for 30 d *in vitro*, scale bar = 100 μm. Quantification of percentage of (**M**) LHX1⁺ and FOXP2⁺ cells, (**O**) HB9⁺ cells, (**P**) ISL 1⁺ cells, and (**Q**) OLIG2⁺ cells in DAPI⁺ cells.

dorsal differentiation medium, and SAG and LDN-193189 were added to the ventral differentiation medium. Immunofluorescence staining (Fig. 2G, H, Fig. 2L, and Fig. 2N) and Q-PCR analysis (Supplementary Fig. 2A and Supplementary Fig. 2B) showed that spinal cord dorsal or ventral INs appeared after being differentiated for 30 d *in vitro*. There were 10.5% ± 1.5% and 3.9% ± 0.9% of MAP2⁺ cells co-labeled with BRN3A (a marker of spinal cord dorsal INs di1c – di3, diLB – di5) in the dorsal group and ventral group respectively (Fig. 2G, H and I) [19]. About 7.8% ± 0.9% and 4.8% ± 1.2% of MAP2⁺ cells were co-labeled with TLX3 (a marker of spinal cord dorsal INs di3, diLB – di5) in the dorsal group and ventral group respectively (Fig. 2G, H and J) [19]. Furthermore, 17.1% ± 3.9% and 6.8% ± 2.4% of MAP2⁺ cells were co-labeled with LMX1B (a marker of spinal cord dorsal INs diLB - di5) in the dorsal and ventral group separately (Fig. 2G, H and K) [19]. In addition, we found that in the ventral group approximately 22.5% ± 5.6% of cells expressed spinal cord ventral di6 - V1 INs marker LHX1,

and 45.6% ± 10.1% of cells expressed spinal cord ventral V1 INs marker FOXP2 (Fig. 2L and M) [19]. Moreover, MNPs and MNs emerged in the ventral group after 30 d culture. Immunofluorescence staining and quantitative data showed that 9.1% ± 4.9% of cells expressed HB9 (Fig. 2N and O), and 13.1% ± 6.2% expressed ISL 1 (Fig. 2N and P), which are both MNs markers, and 8.4% ± 5.8% of cells expressed OLIG2 (also a marker of MNPs) (Fig. 2N and Q) [19].

We performed whole cell patch clamp recording to determine whether induced spinal cord dorsal and ventral INs were electrophysiologically mature, as illustrated in Supplementary Fig. 2C [39,52]. To test the excitability of these neurons, we first investigated the spontaneous electrical discharge evoked by a series of voltage pulses. The recordings showed that the amplitude of the electrical current of spinal cord ventral INs (about 700 pA) was larger than in spinal cord dorsal INs (about 250 pA). Then we tried to elicit action potential trains by injecting a series of currents into the soma of spinal cord dorsal or

ventral INs. As a result, we only detected sodium and potassium currents instead of action potentials in two groups. This is likely because the currents were too weak in immature neurons to produce action potentials. However, the sodium and potassium currents in the spinal cord ventral INs group were more volatile than in the dorsal INs group. These results demonstrate that hscNPCs could differentiate into spinal cord dorsal or ventral INs *in vitro*, although they were not fully electrophysiologically mature.

3.3. DV-SC survived and gradually matured in the lesion site of rats

To detect the function of DV-SC in SCI, we transplanted DV-SC into rat T8-9 complete spinal cord transection model. Scaffolds loaded with undifferentiated hscNPCs (scaffold + NPCs) were also implanted as a

control (Fig. 3A). Rats in each group were sacrificed at 2 wpi and 2 mpi to detect the survival and differentiation of grafted cells. The results showed that at 2 wpi, $491,011 \pm 212$ grafted GFP $^+$ cells and $580,102 \pm 309$ grafted GFP $^+$ cells survived in the scaffold + NPCs group and scaffold + DV-SC group respectively. At 2 mpi, $205,422 \pm 379$ grafted GFP $^+$ cells and $245,532 \pm 224$ grafted GFP $^+$ cells survived in the scaffold + NPCs group and scaffold + DV-SC group respectively. At 2 wpi, >40% of grafted GFP$^+$ cells were immunostained for TUJ1 and < 15% of GFP$^+$ cells were immunostained for NeuN in both groups (Supplementary Fig. 3). Two months post surgery, about $43.3\% \pm 5.4\%$ and $39.1\% \pm 3.9\%$ of GFP$^+$ grafted cells were co-labeled with TUJ1 in scaffold + NPCs group and in scaffold + DV-SC group respectively (Fig. 3B and C). Moreover, $12.1\% \pm 3.7\%$ of grafted GFP$^+$ cells in scaffold + NPCs group and $16.9\% \pm 4.1\%$ in scaffold + DV-SC group
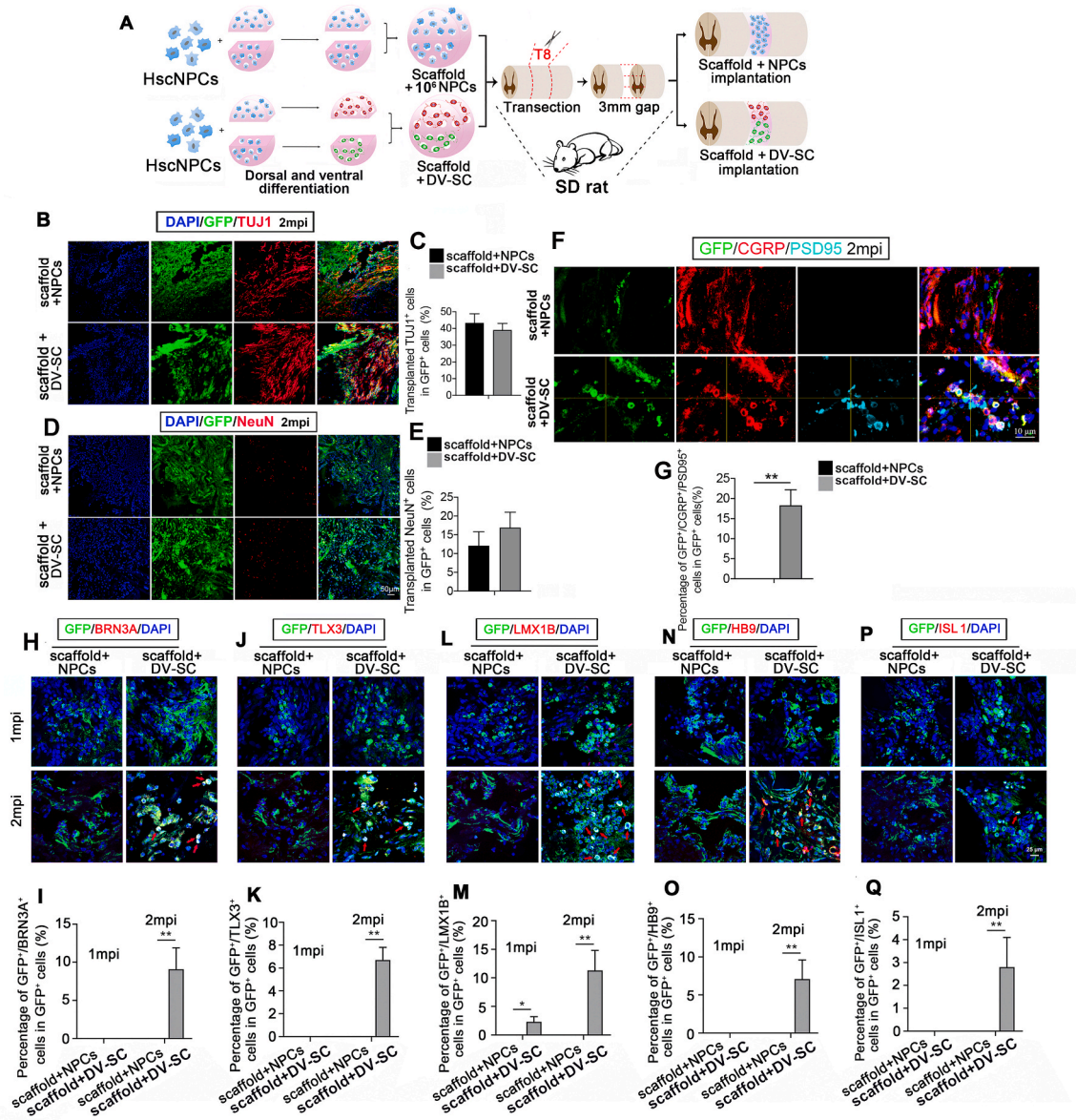

Fig. 3. Transplantation of scaffold + NPCs and scaffold + DV-SC in SCI rats. (**A**) Schematic diagram of the *in vitro* and *in vivo* experimental processes. Immunofluorescence staining of (**B**) TUJ1$^+$ immature neurons and (**D**) NeuN$^+$ mature neurons in the lesion site at 2 mpi. Scale bar = 50 μm. Quantification of percentage of (**C**) GFP$^+$/TUJ1$^+$ cells, and (**E**) GFP$^+$/NeuN$^+$ cells in GFP$^+$ cells. Immunofluorescence staining of (**F**) GFP$^+$/CGRP$^+$/PSD95$^+$ cells in the lesion site at 2 mpi. Scale bar = 10 μm. (**G**) Quantification of the percentage of GFP$^+$/CGRP$^+$/PSD95$^+$ cells in GFP$^+$ cells. **p < 0.01. Immunofluorescence staining of grafted cells differentiated into spinal cord dorsal INs (**H**) BRN3A$^+$ cells, (**J**) TLX3$^+$ cells, (**L**) LMX1B$^+$ cells, and (**N**) HB9$^+$ MNs and (**P**) ISL 1$^+$ MNs in the lesion site at 2 mpi. Scale bar = 25 μm. Quantification of (**I**) GFP$^+$/BRN3A$^+$ cells, (**K**) GFP$^+$/TLX3$^+$ cells, (**M**) GFP$^+$/LMX1B$^+$ cells, (**O**) GFP$^+$/HB9$^+$ cells and (**Q**) GFP$^+$/ISL 1$^+$ cells in GFP$^+$ cells in the lesion site. *p < 0.05, **p < 0.01.

differentiated into mature neurons labeled for NeuN (Fig. 3D and E).

We further investigated whether these mature neurons maintained spinal cord dorsal or ventral INs identities *in vivo*. We found that a few spinal cord dorsal INs or MNs could be detected in the lesion area in the scaffold + DV-SC group at 2 mpi. Immunofluorescence staining and quantitative data illustrated that there were 9.1% $\pm$ 2.8% of GFP$^+$/BRN3A$^+$ cells (spinal cord dorsal di1c – di3, diLB – di5 INs) (Fig. 3H and I), 6.7% $\pm$ 1.1% of GFP$^+$/TLX3$^+$ cells (spinal cord dorsal di3, diLB – di5 INs) (Fig. 3J and K), 11.3% $\pm$ 3.5% of GFP$^+$/LMX1B$^+$ cells (spinal cord dorsal diL$_B$ – di5 INs) (Fig. 3L and M), 7.1% $\pm$ 2.5% of GFP$^+$/HB9$^+$ cells (MNs) (Fig. 3N and O), and 2.8% $\pm$ 1.3% of GFP$^+$/ISL 1$^+$ cells (MNs) (Fig. 3P and Q) in GFP$^+$ grafted cells identified in the lesion area in the scaffold + DV-SC group. It was significantly higher than that in the scaffold + NPCs group.

We also tested the number of CGRP$^+$ and 5-HT$^+$ nerve fibers, and synapse formation in the lesion area in both groups. Immunofluorescence staining results revealed that several GFP$^+$ grafted cells formed contacts with host CGRP$^+$/GFP$^-$ axons in the scaffold + DV-SC group, and some of these cells were PSD95$^+$ (18.3% $\pm$ 3.9%), suggesting synaptic connections between the DV-SC and host axons, however, there were no GFP$^+$/CGRP$^+$/PSD95$^+$ axons in the scaffold + NPCs group (Fig. 3F and G, p < 0.01). Additionally, we found that 5-HT$^+$ nerve fibers rarely extended into the lesion site in both groups. These data indicate that grafted DV-SC can survive and differentiate into mature neurons with spinal cord dorsal and ventral INs identities in rat lesion region at 2 mpi.

3.4. DV-SC graft promoted electrophysiological and motor function recovery in SCI rats

Fig. 4A was the schematic diagram of electrophysiological test. The CMEPs results demonstrated that responsive waves already emerged in rats with only collagen scaffold implantation after SCI (Fig. 4B, blue line).The latent period of scaffold + DV-SC group (6.38 $\pm$ 0.13 m s) was longer than that in the scaffold + NPCs group (5.28 $\pm$ 0.05 m) (Fig. 4C). However, the amplitude of the hindleg in the scaffold + DV-SC group (0.38 $\pm$ 0.2 mV) (Fig. 4D) was statistically larger than in the scaffold + NPCs group (0.14 $\pm$ 0.02 mV) (p < 0.001) or the scaffold group (0.03 $\pm$ 0.01 mV) (p < 0.001).

Recovery of hindlimb motor function was evaluated by BBB score.

We observed that at 2 mpi in the scaffold + DV-SC group, the BBB score (6.7 $\pm$ 0.9) (Fig. 4E, Supplementary Video S1) was significantly higher than in the scaffold + NPCs group (5.3 $\pm$ 0.5) (p < 0.05). This means that rats with DV-SC implantation could almost move all three large hindlimb joints (hip, knee, and ankle), while rats with undifferentiated NPCs implantation could move only one large joint.

Supplementary data related to this article can be found at https://doi .org/10.1016/j.bioactmat.2023.03.015.

3.5. DV-SC survived, matured, and formed synapses with host motor and sensory axons in injured spinal cord of rhesus monkeys

Considering monkeys are more similar to humans than rats, we also transplanted DV-SC or undifferentiated hscNPCs into T8-9 spinal cord transection model of rhesus monkeys. The schematic diagram of transplantation was demonstrated in Fig. 5A. Rhesus monkeys in the scaffold + DV-SC group were sacrificed at 7 dpi, 20 dpi, 2 mpi, 4 mpi, and 6 mpi to detect the survival and differentiation of grafted cells. To enhance the survival and neuronal differentiation of grafted cells in monkeys, we increased the number of transplanted cells and applied triple-drug immunosuppression. The results showed that at 2 mpi, 5,123,208 $\pm$ 2519 grafted GFP $^+$ cells and 6,061,300 $\pm$ 1317 grafted GFP $^+$ cells survived in the scaffold + NPCs group and scaffold + DV-SC group respectively. At 6 mpi, 2,319,500 $\pm$ 2137 grafted GFP $^+$ cells and 2,632,625 $\pm$ 1510 grafted GFP $^+$ cells survived in the scaffold + NPCs group and scaffold + DV-SC group respectively. Immunofluorescence staining analysis and quantitative analysis demonstrated that at 2 mpi, there were 40.1% $\pm$ 9.8% and 30.5% $\pm$ 5.5% of grafted GFP$^+$ cells still expressed TUJ1 in the damage zone in scaffold + NPCs group and scaffold + DV-SC group, respectively (Supplementary Fig. 4A and Supplementary Fig. 4B). However, the percentage of TUJ1$^+$ neurons in grafted GFP$^+$ cells decreased in both groups at 6 mpi, and the percentage of transplanted TUJ1$^+$ cells in GFP$^+$ cells was 28.1% $\pm$ 4.9% and 12.8% $\pm$ 3.5% in the scaffold + NPCs and scaffold + DV-SC groups, respectively (Fig. 5B and C, p < 0.05). Similarly, the percentage of transplanted NeuN$^+$ mature neurons in GFP$^+$ cells increased from 2 mpi to 6 mpi in both groups. At 2 mpi, 9.1% $\pm$ 3.2% and 15.1% $\pm$ 2.9% of grafted GFP$^+$ cells were positively immunostained for NeuN in the damage zone in the scaffold + NPCs and scaffold + DV-SC groups, respectively (Supplementary Fig. 4C and Supplementary Fig. 4D). With the continued
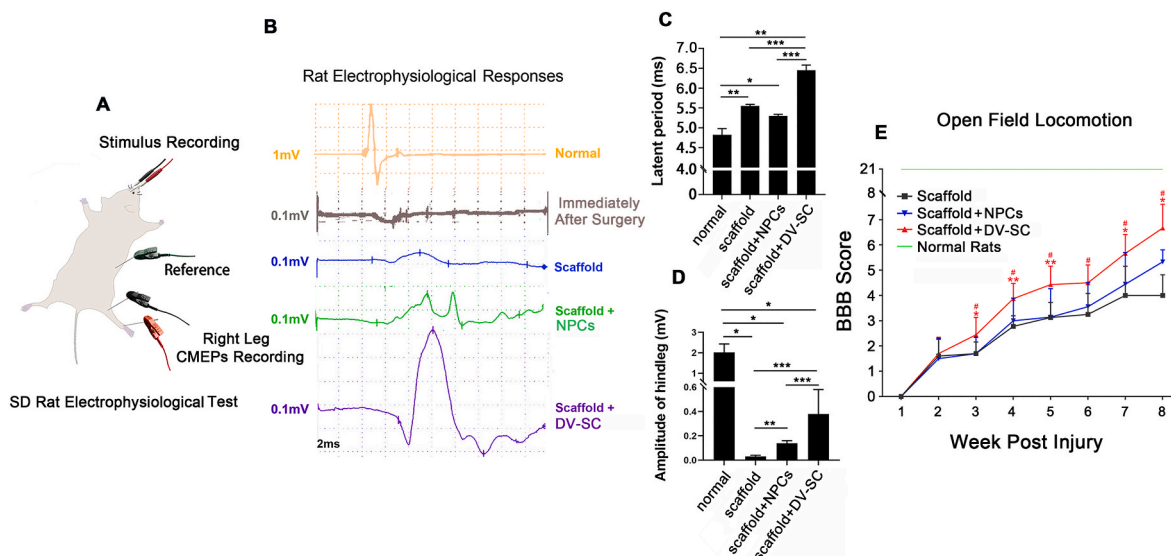

Fig. 4. Transplantation of scaffold + DV-SC promoted electrophysiological and motor function recovery in SCI rats. (**A**) Schematic diagram of rat CMEPs evaluation. (**B**) Waves of CMEPs of rats in each group after 2 mpi. (**C**) Latent periods and (**D**) amplitude of waves in each group at 2 mpi. *p < 0.05, **p < 0.01, ***p < 0.001. (**E**) BBB score of rats in each group at 2 mpi. #p < 0.05 compared with the scaffold group, *p < 0.05 compared with the scaffold + NPCs group, **p < 0.01 compared with the scaffold + NPCs group.
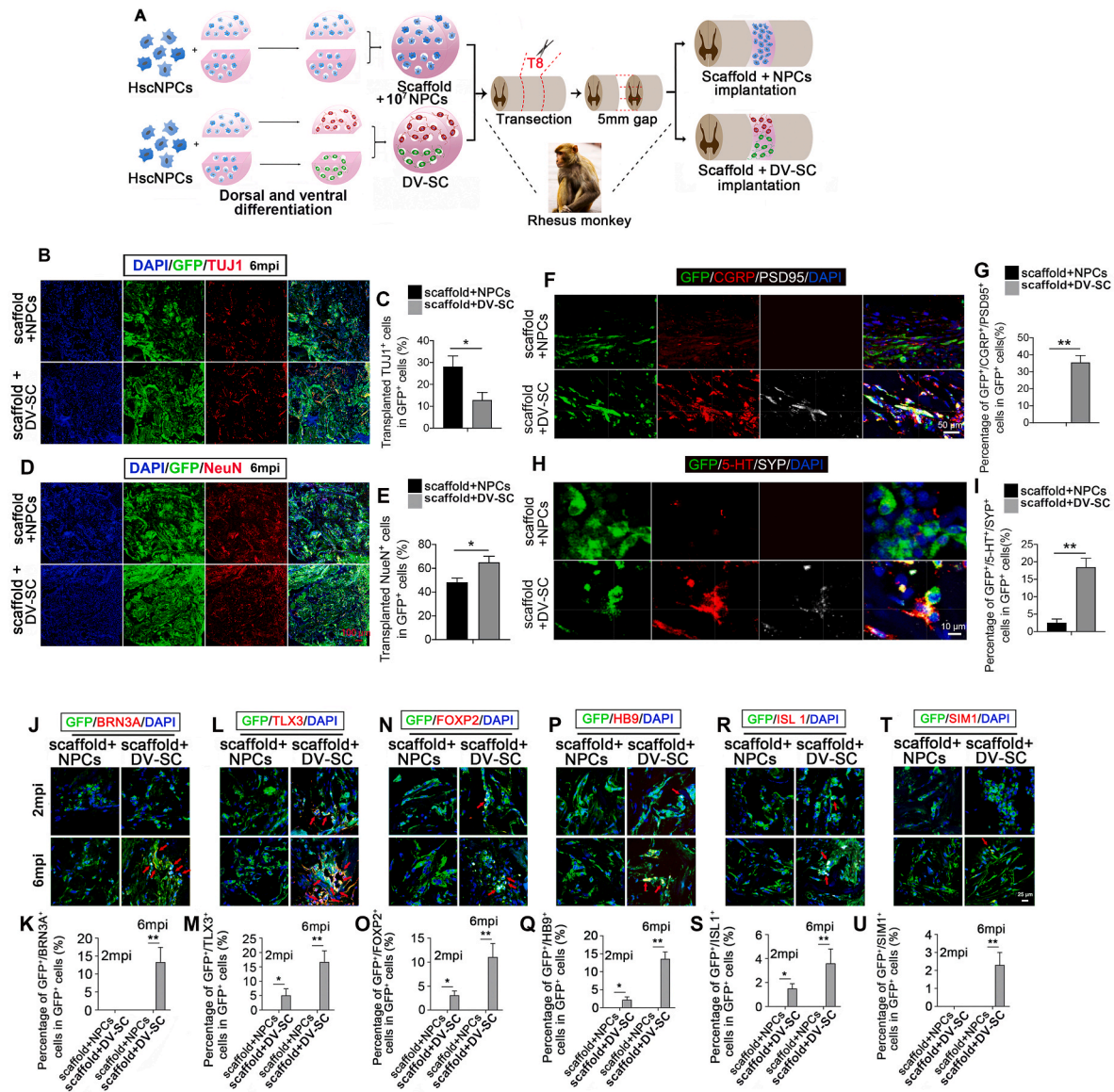
Fig. 5. Transplantation of scaffold + NPCs and scaffold + DV-SC in rhesus monkeys. (**A**) The experimental schematic diagram of the *in vitro* and *in vivo* processes. Immunofluorescence staining of grafted cells differentiated into (**B**) TUJ1$^+$ immature neurons and (**D**) NeuN$^+$ mature neurons in the lesion site at 6 mpi. Scale bar = 100 μm. Quantification of (**C**) percentage of GFP$^+$/TUJ1$^+$ cells in GFP$^+$ cells. *p < 0.05. and (**E**) percentage of GFP$^+$/NeuN$^+$ cells in GFP$^+$ cells. *p < 0.05. Immunofluorescence staining of (**F**) GFP$^+$/CGRP$^+$/PSD95$^+$ cells, scale bar = 50 μm, and (**H**) GFP$^+$/5-HT$^+$/SYP$^+$ cells in the lesion site at 6 mpi. Scale bar = 10 μm. Quantification of the percentage of (**G**) GFP$^+$/CGRP$^+$/PSD95$^+$ cells and (**I**) GFP$^+$/5-HT$^+$/SYP$^+$ cells in GFP$^+$ cells. **p < 0.01. Immunofluorescence staining of grafted cells differentiated into spinal cord dorsal INs (**J**) GFP$^+$/BRN3A$^+$ cells, (**L**) GFP$^+$/TLX3$^+$ cells, or spinal cord ventral INs (**N**) GFP$^+$/FOXP2$^+$ cells, (**T**) GFP$^+$/SIM1$^+$cells, or MNs (**P**) GFP$^+$/HB9$^+$ cells, (**R**) GFP$^+$/ISL 1$^+$ cells in the lesion site at 6 mpi. Scale bar = 25 μm. Quantification of percentage of (**K**) GFP$^+$/BRN3A$^+$ cells, (**M**) GFP$^+$/TLX3$^+$ cells, (**O**) GFP$^+$/FOXP2$^+$ cells, (**U**) GFP$^+$/SIM1$^+$cells, (**Q**) GFP$^+$/HB9$^+$ cells, and (**S**) GFP$^+$/ISL 1$^+$ cells in GFP$^+$ cells. *p < 0.05, **p < 0.01.

maturation of grafted GFP$^+$ cells, the cell percentage increased to 48.2% ± 3.5% and 65.2% ± 5.1% in the scaffold + NPCs group and scaffold + DV-SC group at 6 mpi, respectively (Fig. 5D and E, p < 0.05). Remarkably, a larger proportion of grafted GFP$^+$ cells in the scaffold + DV-SC group differentiated into mature NeuN$^+$ neurons at the damage site compared with the scaffold + NPCs group.

We supplemented with the immunostaining of macrophage/microglia marker CD68 of grafted GFP$^+$ cells in both groups at 6 mpi to show phagocytosis (Supplementary Fig. 5).We observed that only a small number of GFP$^+$ and CD68$^+$ double immunostained cells were in the lesion site in two groups.

Subsequently, we confirmed that mature neurons derived from grafted cells could still keep spinal cord dorsal or ventral INs characteristics in the damage site. Compared with the scaffold + NPCs groups,

a larger number of mature postmitotic spinal cord dorsal and ventral INs were observed in the damage zone at 6 mpi in the scaffold + DV-SC group (Fig. 5J–U). In the scaffold + NPCs group, we found no spinal cord dorsal INs GFP$^+$/BRN3A$^+$ cells or GFP$^+$/TLX3$^+$ cells, whereas a remarkable increase of GFP$^+$/BRN3A$^+$ cells (Fig. 5J and K, 13.3% ± 4.1%, p < 0.01) and GFP$^+$/TLX3$^+$ cells (Fig. 5L and M, 16.7% ± 3.9%, p < 0.01) were observed at the damage site in the scaffold + DV-SC group. Similarly, MNs and spinal cord ventral INs showed a similar trend. Compared with the scaffold + NPCs group, which had no HB9$^+$ or ISL 1$^+$ MNs, 13.6% ± 1.9% of GFP$^+$/HB9$^+$ and 3.6% ± 1.2% of GFP$^+$/ISL 1$^+$ MNs in GFP$^+$ grafted cells were observed in the scaffold + DV-SC group (Fig. 5P and Q, p < 0.01. Fig. 5R and S, p < 0.01). In the scaffold + DV-SC group, 11.1% ± 2.8% of spinal cord ventral neurons GFP$^+$/FOXP2$^+$ V1 INs and 2.3% ± 0.7% of GFP$^+$/SIM1$^+$ V3 INs in GFP$^+$ grafted cells were

found. This was higher than that in the scaffold + NPCs group, which had no GFP$^+$/FOXP2$^+$ or GFP$^+$/SIM1$^+$ cells at the lesion site (Fig. 5N and O, p < 0.01. Fig. 5T and U, p < 0.01). Supplementary Fig. 6 were single channel images of Fig. 5J, L, N, P, R, and T with arrows pointing to the co-staining cells to visualize the marker expression more clearly.

5-HT$^+$ efferents, CGRP$^+$ afferents, and synapse formation in the lesion region were also examined. At 6 mpi, in the scaffold + DV-SC group, 35.3% ± 4.1% of GFP$^+$ donor cells formed PSD95$^+$ synapses with host CGRP$^+$/GFP$^-$ axons, significantly higher than that in the scaffold + NPCs group (Fig. 5F and G, p < 0.01). Furthermore, in the scaffold + DV-SC group, we observed there were some 5-HT$^+$ nerve fibers at the lesion site, and some SYP$^+$ synapses formed between them and the GFP$^+$ donor cells (18.5% ± 2.5%) (Fig. 5H and I), however, in the scaffold + NPCs group, a few 5-HT$^+$ nerve fibers extended into the injury center (Fig. 5H and I, 2.5% ± 1.1%, p < 0.01). In addition, we found that a small number of BRN3A$^+$ neurons derived from grafted GFP$^+$ cells contacted with host GFP$^-$/CGRP$^+$ axons in the lesion site in the scaffold + DV-SC group at 6 mpi (Supplementary Fig. 7).

To further demonstrate tissue remodeling and collagen scaffold degradation, we have supplemented with histological analysis for H&E and Picrosirus Red for collagen in the scaffold + DV-SC group in monkeys at different time point after implantation (Supplementary Fig. 8A and Supplementary Fig. 8B). The results demonstrated that the collagen was progressively degraded. For detecting the exogenous GFP$^+$ cells, we used Nissl staining to confirm the existence of neurons in lesion sites (Supplementary Fig. 8C). The results showed that there were more neurons in the lesion site in the scaffold + DV-SC group than in scaffold + NPCs group at 2 mpi, 4 mpi, and 6 mpi (Supplementary Fig. 8D, Supplementary Fig. 8E and Supplementary Fig. 8F). Together with these data, we propose the neural regeneration is accompanied by matrix degradation, which is a typical phenomenon for tissue repair.

These results demonstrated that grafted DV-SC could survive and differentiate into mature neurons that still possessed spinal cord dorsal and ventral INs characteristics in SCI lesions of rhesus monkeys at 6 mpi. DV-SC could also form synapses with host motor and sensory axons in injured spinal cord of rhesus monkeys.

3.6. DV-SC graft prominently improved electrophysiological and motor function recovery in SCI rhesus monkeys

We also assessed SCMEPs and hindlimb motor function recovery in rhesus monkeys. The amplitude of a normal SCMEPs wave was approximately 78 μV (Fig. 6B). Until the end of the observation period, SCMEPs responses were discovered in two rhesus monkeys. One was in

the subject F7 rhesus monkey, with an amplitude similar to the normal wave; the other was in the subject F11 rhesus monkey, with an amplitude that was approximately 41 μV in the scaffold + DV-SC group at 6 mpi (Fig. 6B). These responses were not observed in the scaffold + NPCs group (Fig. 6B).

The hindlimb movement abilities in DV–SC–implanted rhesus monkeys were continuously observed during the experimental period. At 6 mpi, the muscle strength of the hindlimb was partially restored, and one rhesus monkey (F11) in the scaffold + DV-SC group (Fig. 6C and Supplementary Video S2) could alternately lift left and right knee joint several times, though its hindlimb joint movements could not be observed at 3 mpi (Supplementary Video S3). The rhesus monkeys in the control group (Fig. 6C and Supplementary Video S4) and the scaffold + NPCs group (Fig. 6C and Supplementary Video S5) were unable to move their hindlimb joints during the entire observation period. These findings reveal that DV-SC transplantation could promote electrophysiological and hindlimb motor function recovery in rhesus monkeys following SCI.

4. Discussion

NPCs-based therapy has been regarded as a promising and potential therapeutic method for treating SCI. However, in SCI animal models, grafted NPCs within the injured area are seldom differentiated into distinct types of functional spinal cord neurons in a short therapeutic window period. In our study, we attempted to pre-differentiate human NPCs *in vitro* to obtain dorsal and ventral spinal cord neuronal progenitors on collagen scaffold before transplantation *in vivo*. The implantation of DV-SC in SCI animals could survive and mature to produce dorsal and ventral functional neurons to promote SCI repair.

We isolated and cultured human spinal cord NPCs from a gestational 7-week-old human embryo spinal cord. This was performed based on one of our published works assessing high-throughput single-cell RNA sequencing for developing the human spinal cord. Seven weeks of gestation is a key time point for transforming neuronal differentiation to astrocytic differentiation [20]. At this time, almost all spinal cord cells are lineage-restricted neuronal progenitors. Astrocyte markers (GFAP and ALDH1L1) do not emerge until after 8 weeks of gestation. These high-purity neuronal progenitors could benefit our subsequent research by producing many spinal cord dorsal and ventral neurons. We propose the plasticity of NPCs isolated from embryo spinal cord before 7 weeks of gestation is appropriate to induce differentiation into distinct subpopulations of neurons.

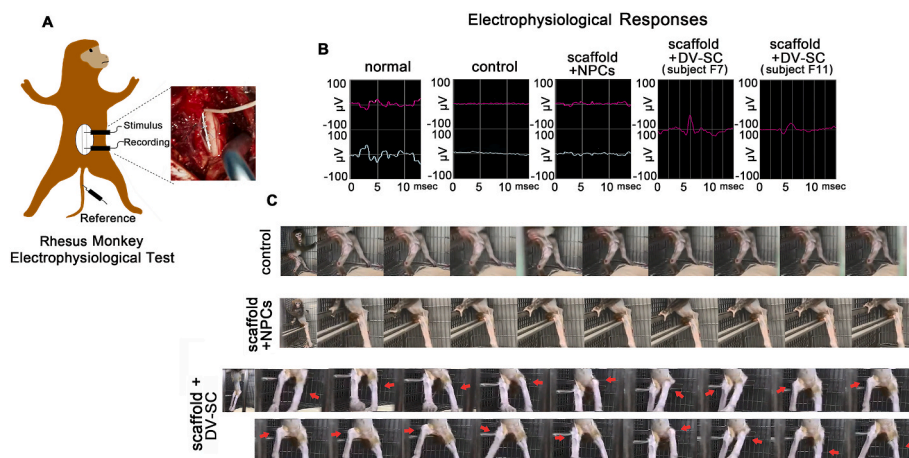In 2018, Dulin et al. demonstrated that injured rat host CGRP$^+$

Fig. 6. Transplantation of scaffold + DV-SC improved electrophysiological and motor function recovery in rhesus monkeys. (**A**) Schematic diagram of rhesus monkey SCMEPs evaluation. (**B**) Waves of SCMEPs of rhesus monkeys in each group after 6 mpi. (**C**) Images of hindlimb joint movements of rhesus monkeys in each group at 6 mpi. Subject F11 rhesus monkey in scaffold + DV-SC group could lift left and right knee joints several times.

sensory axons can selectively innervate graft domains populated with particular dorsal neuronal subtypes and avoid domains filled with inappropriate targets. In their work, grafted NPCs formed a dorsal horn-like structure that contained spinal cord dI4-dI6 neurons identified by LBX1 expression [21,53]. In our work, pre-differentiated dorsal and ventral hscNPCs can generate dorsal and ventral neurons, including BRN3A$^+$ neurons representing spinal cord dorsal di1c - di3, diLB - di5 INs, TLX3$^+$ neurons representing spinal cord dorsal di3, diLB - di5 INs, HB9$^+$ and ISL 1$^+$ MNs, and FOXP2$^+$ neurons representing ventral V1 INs and SIM1$^+$ neurons representing ventral V3 INs. Similarly, we found that host efferents and afferents could target corresponding graft-derived axons; for example, CGRP$^+$ afferents could innervate graft-derived sensory neurons and form synapses. Additionally, host 5-HT$^+$ efferents could innervate graft-derived MNs and form synapses. We thought that the enhancement of electrophysiological results and hindlimb motor functions could be associated with graft integrating into the inherent host spinal cord neural network, which could partially resume interrupted spinal cord neural circuitry in the damaged area.

Similar with many studies for NPCs transplantation [54], the grafted cells tended to disperse into the surrounding normal spinal tissue and rarely retain at injured sites because of the flow of cerebrospinal fluid. It might be also related to the adequate nutrition of spared tissues mobilize the implanted cells towards the spared tissues. We propose the GFP cells in the spared tissue also contribute to the recovery of SCI animals, because SCI often leads to the degenerative microenvironment in the distal sites of spinal cords.

We found that grafted cells within an injured area in rats or rhesus monkeys differentiated into fewer neurons *in vivo* than *in vitro*. When differentiated *in vitro* for 30 d, about 50% of hscNPCs could become mature MAP2$^+$ spinal cord dorsal INs, and 70% of hscNPCs could become MAP2$^+$ ventral INs. However, when transplanted *in vivo*, the percentage of graft-derived mature spinal cord dorsal and ventral INs was lower. Less than 20% of grafted pre-differentiated dorsal and ventral hscNPCs differentiated into mature NeuN $^+$ neurons in rats or monkeys at 2 mpi. Compared with an *in vitro* environment, injured myelin-forming oligodendrocytes in the lesion area release a mass of myelin-associated proteins, such as Nogo, myelin-associated glycoprotein, and oligodendrocyte myelin glycoprotein [55,56]. Nogo, myelin-associated glycoprotein, and oligodendrocyte myelin glycoprotein reportedly play crucial roles in inhibiting axon regeneration and the neuronal differentiation of NSPCs by activating the epidermal growth factor receptor signaling pathway [13,15,57,58]. In addition, ischemia and oxidative stress after SCI contribute to a cascade of inflammation, excitotoxicity, and enzyme inactivation during the secondary injury phase, which can lead to neuronal death [59]. For this reason, providing exogenous delivery of chemotrophic neurotrophic protein factors could be important in future work for improving the neuronal differentiation of grafted cells.

Compared with transplantation into SCI rats, more grafted cells differentiated towards mature neurons in SCI rhesus monkeys. We attributed this to two reasons. First, this could be associated with more grafted hscNPCs (10^7 cells) being grafted in rhesus monkeys than (10^6) in rats. Lu et al. demonstrated that engrafted NSPCs could naturally secrete significant quantities of several neurotrophic factors, including nerve growth factor (NGF), BDNF, and GDNF [60]. NGF combined with BDNF can remarkably improve NSPC neuronal differentiation [61–65], and GDNF has also been reported to have a positive effect on neuronal differentiation of NSPCs [66–68]. Therefore, more grafted hscNPCs can secrete more neurotrophic factors, which helps generate more mature neurons in rhesus monkeys than in rats. Second, to increase the graft survival rate, we increased the size of the collagen scaffold to 7 mm × 8 mm × 4 mm to seed more hscNPCs and applied more immunosuppression. Using these methods, more grafted neuronal-restricted progenitors can survive in the injured spinal cord.

Synapse formation is very important for the function of DV-SC. First, the diverse types of neurons in DV-SC might be crucial for forming functional synapse. It might be related to the more neuronal circuit formation by different INs and MNs in DV-SC compared to undifferentiated NPCs. Second, DV-SC might produce more neurotrophic factors than undifferentiated NPCs due to they differentiate into mature neurons. Neurotrophic factors also potentiate synapse formation between grafted DV-SC donors and host 5-HT$^+$ or CGRP$^+$ axons, such as BDNF [69], NGF [70] and GDNF [71]. As a result, DV-SC could establish more synaptic contacts with host nerve axons than undifferentiated NPCs.

In conclusion, our work demonstrated that after transplanting pre-differentiated dorsal and ventral hscNPCs into rat or rhesus monkey T8-9 spinal cord transected injury models, grafts could differentiate into mature neurons and maintain their spinal cord dorsal and ventral neurons identities. Several 5-HT$^+$ motor axonal efferents and CGRP$^+$ sensory axonal afferents were observed in the injured area of rhesus monkeys. Host 5-HT$^+$ axons and CGRP$^+$ axons separately came into contact with graft-derived motor axons and sensory axons and formed synapses with them. Grafts integrated into host nerve fibers could contribute to partially recovering interrupted neuronal circuits, thus promoting SCI animals' electrophysiological signaling and hindlimb motor function recovery. Our findings suggest that transplantation of pre-differentiated dorsal and ventral hscNPCs could provide a reference for supporting the better assembly of new neuronal circuits and gaining greater functional recovery in future work on SCI translation.

5. Conclusions

In conclusion, our work demonstrated that after transplanting DV-SC into rat or rhesus monkey T8-9 spinal cord transected injury models, grafts could differentiate into mature neurons and maintain their spinal cord dorsal and ventral neurons identities. Several 5-HT + motor axonal efferents and CGRP + sensory axonal afferents were observed in injured areas of rhesus monkeys. Host 5-HT$^+$ axons and CGRP$^+$ axons came into contact with graft-derived motor axons and sensory axons separately and formed synapses. Grafts integrated into host nerve fibers could contribute to partially recovering interrupted neuronal circuits, thus promoting SCI electrophysiological signaling and hindlimb motor function recovery in certain animals.

Ethics

Rats were supplied and housed at the experimental animal center at the Institute of Genetics and Developmental Biology, Chinese Academy of Sciences (Bejing, China), and all surgeries were performed there. Rhesus monkeys were supplied and housed at the experimental animal center in Hunan Puruima Medicine Research Center (Hunan, China), and all surgeries were performed there. All experimental and surgical procedures were performed in accordance with the Chinese Ministry of Public Health Guide and were approved by the Institutional Animal Care and Use Committee of Hunan Puruima Medicine Research Center.

The use of human embryo tissues for cell culturing was approved by the Reproductive Study Ethics Committee of Nanjing Drum Tower Hospital and Nanjing Medical University (2018-223-01). Informed consent was provided by the donors. The aborted embryo tissues were acquired from legally terminated pregnancies.

CRediT authorship contribution statement

Bai Xu: Conceptualization, Methodology, Investigation, Writing – original draft, revision & editing. **Dingyang Liu:** Methodology, Investigation, Visualization. **Weiyuan Liu:** Methodology, Investigation, Visualization. **Ge Long:** Investigation. **Wenbin Liu:** Resources. **Yayu Wu:** Resources, Investigation. **Xinghui He:** Investigation. **Yeyu Shen:** Investigation. **Peipei Jiang:** Resources. **Man Yin:** Resources, Investigation. **Yongheng Fan:** Resources, Investigation. **He Shen:** Supervision. **Liyang Shi:** Conceptualization, revision & editing, Supervision. **Qi Zhang:** Data curation. **Weiwei Xue:** Data curation. **Chen Jin:** Data

curation. **Zhenni Chen:** Data curation. **Bing Chen:** Supervision. **Jiayin Li:** Supervision. **Yali Hu:** Resources. **Xing Li:** Conceptualization, revision & editing, Supervision. **Zhifeng Xiao:** Conceptualization, revision & editing, Supervision. **Yannan Zhao:** Conceptualization, revision & editing, Supervision. **Jianwu Dai:** Conceptualization, Supervision, Funding acquisition.

Declaration of competing interest

The authors declare that they have no known competing financial interests or personal relationships that could have appeared to influence the work reported in this paper.

Acknowledgments

Appendix A. Supplementary data

Supplementary data to this article can be found online at https://doi.org/10.1016/j.bioactmat.2023.03.015.

References

[1] J.W. McDonald, C. Sadowsky, Spinal-cord injury, Lancet 359 (9304) (2002) 417–425.
[2] B.B. Lee, R.A. Cripps, M. Fitzharris, P.C. Wing, The global map for traumatic spinal cord injury epidemiology: update 2011, global incidence rate, Spinal Cord 52 (2) (2014) 110–116.
[3] E. Akesson, E. Sundström, Human neural progenitor cells in central nervous system lesions, Best Pract. Res. Clin. Obstet. Gynaecol. 31 (2016) 69–81.
[4] X.Y. Lin, B.Q. Lai, X. Zeng, M.T. Che, E.A. Ling, W.T. Wu, Y.S. Zeng, Cell transplantation and neuroengineering approach for spinal cord injury treatment: a summary of current laboratory findings and review of literature, Cell Transplant. 25 (8) (2016) 1425–1438.
[5] M.A. Lane, A.C. Lepore, I. Fischer, Improving the therapeutic efficacy of neural progenitor cell transplantation following spinal cord injury, Expert Rev. Neurother. 17 (5) (2017) 433–440.
[6] P. Assinck, G.J. Duncan, B.J. Hilton, J.R. Plemel, W. Tetzlaff, Cell transplantation therapy for spinal cord injury, Nat. Neurosci. 20 (5) (2017) 637–647.
[7] I. Fischer, J.N. Dulin, M.A. Lane, Transplanting neural progenitor cells to restore connectivity after spinal cord injury, Nat. Rev. Neurosci. 21 (7) (2020) 366–383.
[8] K. Yamazaki, M. Kawabori, T. Seki, K. Houkin, Clinical trials of stem cell treatment for spinal cord injury, Int. J. Mol. Sci. 21 (11) (2020) 3994.
[9] T. Bedir, S. Ulag, C.B. Ustundag, O. Gunduz, 3D bioprinting applications in neural tissue engineering for spinal cord injury repair, Mater Sci Eng C Mater Biol Appl 110 (2020), 110741.
[10] X.C. Hu, Y.B. Lu, Y.N. Yang, X.W. Kang, Y.G. Wang, B. Ma, S. Xing, Progress in clinical trials of cell transplantation for the treatment of spinal cord injury: how many questions remain unanswered? Neural Regen Res 16 (3) (2021) 405–413.
[11] V. Kottis, P. Thibault, D. Mikol, Z.C. Xiao, R.L. Zhang, P. Dergham, Oligodendrocyte-myelin glycoprotein (OMgp) is an inhibitor of neurite outgrowth, J. Neurochem. 82 (6) (2002) 1566–1569.
[12] A.W. McGee, S.M. Strittmatter, The Nogo-66 receptor: focusing myelin inhibition of axon regeneration, Trends Neurosci. 26 (4) (2003) 193–198.
[13] B. Wang, Z.F. Xiao, B. Chen, J. Han, Y. Gao, J. Zhang, W.X. Zhao, X. Wang, J. W. Dai, Nogo-66 promotes the differentiation of neural progenitors into astroglial lineage cells through mTOR-STAT3 pathway, PLoS One 3 (3) (2008), e1856.
[14] V. Neirinckx, D. Cantinieaux, C. Coste, B. Rogister, R. Franzen, S.W. Geebebien, Concise review: spinal cord injuries: how could adult mesenchymal and neural crest stem cells take up the challenge? Stem Cell. 32 (4) (2014) 829–843.
[15] X.R. Li, Z.F. Xiao, J. Han, L. Chen, H.S. Xiao, F.K. Ma, X.L. Hou, X. Li, J. Sun, W. Y. Ding, Y.N. Zhao, B. Chen, J.W. Dai, Promotion of neuronal differentiation of neural progenitor cells by using EGFR antibody functionalized collagen scaffolds for spinal cord injury repair, Biomaterials 34 (21) (2013) 5107–5116.
[16] P. Lu, K. Kadoya, M.H. Tuszynski, Axonal growth and connectivity from neural stem cell grafts in models of spinal cord injury, Curr. Opin. Neurobiol. 27 (2014) 103–109.
[17] B.Y. Fan, Z.J. Wei, X. Yao, G.D. Shi, X. Cheng, X.H. Zhou, H.X. Zhou, G.Z. Ning, X. H. Kong, S.Q. Feng, Microenvironment imbalance of spinal cord injury, Cell Transplant. 27 (6) (2018) 853–866.
[18] X.R. Li, C.X. Fan, Z.F. Xiao, Y.N. Zhao, H.M. Zhang, J. Sun, Y. Zhuang, X.M. Wu, J. J. Shi, Y.Y. Chen, J.W. Dai, A collagen microchannel scaffold carrying paclitaxel-liposomes induces neuronal differentiation of neural stem cells through Wnt/β-catenin signaling for spinal cord injury repair, Biomaterials 183 (2018) 114–127.
[19] W.A. Alaynick, T.M. Jessell, S.L. Pfaff, Snapshot: spinal cord development, Cell 146 (1) (2011), 178-178. e1.
[20] Q. Zhang, X.M. Wu, Y.H. Fan, P.P. Jiang, Y.N. Zhao, Y.M. Yang, S.F. Han, B. Xu, B. Chen, J. Han, M.H. Sun, G.F. Zhao, Z.F. Xiao, Y.L. Hu, J.W. Dai, Single-cell analysis reveals dynamic changes of neural cells in developing human spinal cord, EMBO Rep. 22 (11) (2021), e52728.
[21] J.N. Dulin, A.F. Adler, H. Kumamaru, G.H.D. Poplawski, C.L. Kubli, H. Strobl, D. Gibbs, K. Kadoya, J.W. Fawcett, P. Lu, M.H. Tuszynski, Injured adult motor and sensory axons regenerate into appropriate organotypic domains of neural progenitor grafts, Nat. Commun. 9 (1) (2018) 84.
[22] P. Lu, Y.Z. Wang, L. Graham, K. McHale, M.Y. Gao, D. Wu, J. Brock, A. Blesch, E. S. Rosenzweig, L.A. Havton, B.H. Zheng, J.M. Conner, M. Marsala, M.H. Tuszynski, Long-distance growth and connectivity of neural stem cells after severe spinal cord injury, Cell 150 (6) (2012) 1264–1273.
[23] P. Lu, G. Woodruff, Y.Z. Wang, L. Graham, M. Hunt, D. Wu, E. Boehle, R. Ahmad, G. Poplawski, J. Brock, L.S.B. Goldstein, M.H. Tuszynski, Long-distance axonal growth from human induced pluripotent stem cells after spinal cord injury, Neuron 83 (4) (2014) 789–796.
[24] K. Kadoya, P. Lu, K. Nguyen, C.L. Kubli, H. Kumamaru, L. Yao, J. Knackert, G. Poplawski, J.N. Dulin, H. Strobl, Y. Takashima, J. Biane, J. Conner, S.C. Zhang, M.H. Tuszynski, Spinal cord reconstitution with homologous neural grafts enables robust corticospinal regeneration, Nat. Med. 22 (5) (2016) 479–487.
[25] P. Lu, S. Ceto, Y.Z. Wang, L. Graham, D. Wu, H. Kumamaru, E. Staufenberg, M. H. Tuszynski, Prolonged human neural stem cell maturation supports recovery in injured rodent CNS, J. Clin. Invest. 127 (9) (2017) 3287–3299.
[26] H. Kumamaru, K. Kadoya, A.F. Adler, Y. Takashima, L. Graham, G. Coppola, M. H. Tuszynski, Generation and post-injury integration of human spinal cord neural stem cells, Nat. Methods 15 (9) (2018) 723–731.
[27] B.K. Kwon, F. Streijger, C.E. Hill, A.J. Anderson, M. Bacon, M.S. Beattie, A. Blesch, E.J. Bradbury, A. Brown, J.C. Bresnahan, C.C. Case, R.W. Colburn, S. David, J. W. Fawcett, A.R. Ferguson, I. Fischer, C.L. Floyd, J.C. Gensel, J.D. Houle, L. B. Jakeman, N.D. Jeffery, L.A.T. Jones, N. Kleitman, J.D. Kocsis, P. Lu, D.S. K. Magnuson, M. Marsala, S.W. Moore, A.J. Mothe, M. Oudega, G.W. Plant, A. S. Rabchevsky, J.M. Schwab, O. Steward, X.M. Xu, J.D. Guest, W. Tetzlaff, Large animal and primate models of spinal cord injury for the testing of novel therapies, Exp. Neurol. 269 (2015) 154–168.
[28] W.Y. Liu, B. Xu, S.J. Zhao, S.Y. Han, R. Quan, W.B. Liu, C.N. Ji, B. Chen, Z.F. Xiao, M. Yin, Y.Y. Yin, J.W. Dai, Y.N. Zhao, Spinal cord tissue engineering via covalent interaction between biomaterials and cells, Sci. Adv. 9 (6) (2023), eade8829.
[29] B. Xu, M. Yin, Y.M. Yang, Y.L. Zou, W.B. Liu, L.Y. Qiao, J.X. Zhang, Z. Wang, Y. Y. Wu, H. Shen, M.H. Sun, W.Y. Liu, W.W. Xue, Y.H. Fan, Q. Zhang, B. Chen, X. M. Wu, Y. Shi, F.L. Lu, Y.N. Zhao, Z.F. Xiao, J.W. Dai, Transplantation of neural stem progenitor cells from different sources for severe spinal cord injury repair in rat, Bioact. Mater. 23 (23) (2022) 300–313.
[30] C. Jin, Y.Y. Wu, H.P. Zhang, B. Xu, W.B. Liu, C.N. Ji, P.P. Li, Z.N. Chen, B. Chen, J. Y. Li, X.M. Wu, P.P. Jiang, Y.L. Hu, Z.F. Xiao, Y.N. Zhao, J.W. Dai, Spinal cord tissue engineering using human primary neural progenitor cells and astrocytes, Bioeng Transl Med (2022), e10448.
[31] T.M. Jessell, Neuronal specification in the spinal cord: inductive signals and transcriptional codes, Nat. Rev. Genet. 1 (1) (2000) 20–29.
[32] J.R. Timmer, C. Wang, L. Niswander, BMP signaling patterns the dorsal and intermediate neural tube via regulation of homeobox and helix-loop-helix transcription factors, Development 129 (10) (2002) 2459–2472.
[33] V.V. Chizhikov, K.J. Millen, Mechanisms of roof plate formation in the vertebrate CNS, Nat. Rev. Neurosci. 5 (10) (2004) 808–812.
[34] M. Goulding, Circuits controlling vertebrate locomotion: moving in a new direction, Nat. Rev. Neurosci. 10 (7) (2009) 507–518.
[35] D.C. Lu, T.Y. Niu, W.A. Alaynick, Molecular and cellular development of spinal cord locomotor circuitry, Front. Mol. Neurosci. 8 (2015) 25.
[36] J.B. Bikoff, Interneuron diversity and function in the spinal motor system, Curr. Opin.Physiol. 8 (2019) 36–43.
[37] M.M. Zavvarian, J. Hong, M.G. Fehlings, The functional roles of spinal interneurons following traumatic spinal cord injury, Front. Cell. Neurosci. 14 (2020) 127.
[38] J. Moini, P. Piran, Functional and Clinical Neuroanatomy, Academic Press, 2019.
[39] X.F. Guo, K. Johe, P. Molnar, H. Davis, J. Hickman, Characterization of a human fetal spinal cord stem cell line, NSI-566RSC, and its function to functional motoneurons, J Tissue Eng Regen Med 4 (3) (2010) 181–193.
[40] P.M. Jordan, L.D. Ojeda, J.R. Thonhoff, J.L. Gao, D. Boehning, Y.J. Yu, P. Wu, Generation of spinal MNs from human fetal brain-derived neural stem cells: role of basic fibroblast growth factor, J. Neurosci. Res. 87 (2) (2009) 318–332.
[41] A. Bhinge, S.C. Namboori, A. Bithell, C. Soldati, N.J. Buckley, L.W. Stanton, MiR-375 is essential for human spinal motor neuron development and may be involved in motor neuron degeneration, Stem Cell. 34 (1) (2016) 124–134.
[42] J. Kawada, S. Kaneda, T. Kirihara, A. Maroof, T. Levi, K. Eggan, T. Fujii, Y. Ikeuchi, Generation of a motor nerve organoid with human stem cell-derived neurons, Stem Cell Rep. 9 (5) (2017) 1441–1449.
[43] S. Gao, X.X. Guo, S.M. Zhao, Y.P. Jin, F. Zhou, P. Yuan, L.M. Cao, J. Wang, Y. Qiu, C.X. Sun, Z.R. Kang, F.J. Gao, W. Xu, X. Hu, D.J. Yang, Y. Qin, K. Ning, P.J. Shaw, G.S. Zhong, L.M. Cheng, H.W. Zhu, Z.L. Gao, X. Chen, J. Xu, Differentiation of human adipose-derived stem cells into neuron/motoneuron-like cells for cell replacement therapy of spinal cord injury, Cell Death Dis. 10 (8) (2019) 597.

[44] Y.L. Zou, D.Z. Ma, H. Shen, Y.N. Zhao, B. Xu, Y.H. Fan, Z. Sun, B. Chen, W.W. Xue, Y. Shi, Z.F. Xiao, R. Gu, J.W. Dai, Aligned collagen scaffold combination with human spinal cord-derived neural stem cells to improve spinal cord injury repair, Biomater. Sci. 8 (18) (2020) 5145–5156.

[45] B. Xu, Y.N. Zhao, Z.F. Xiao, B. Wang, H. Liang, X. Li, Y.X. Fang, S.F. Han, X.R. Li, C. X. Fan, J.W. Dai, A dual functional scaffold tethered with EGFR antibody promotes neural stem cell retention and neuronal differentiation for spinal cord injury repair, Adv Healthc Mater 6 (9) (2017).

[46] S.F. Han, W. Yin, X. Li, S.Y. Wu, Y.D. Cao, J. Tan, Y.N. Zhao, X.L. Hou, L. Wang, C. P. Ren, J. Li, X. Hu, Y. Mao, G. Li, B. Li, H.P. Zhang, J. Han, B. Chen, Z.F. Xiao, X. J. Jiang, J.W. Dai, Pre-clinical evaluation of CBD-NT3 modified collagen scaffolds in completely spinal cord transected non-human primates, J. Neurotrauma 36 (15) (2019) 2316–2324.

[47] S.F. Han, Z.F. Xiao, X. Li, H. Zhao, B. Wang, Z.X. Qiu, Z. Li, X. Mei, B. Xu, C.X. Fan, B. Chen, J. Han, Y.Z. Gu, H.L. Yang, Q. Shi, J.W. Dai, Human placenta-derived mesenchymal stem cells loaded on linear ordered collagen scaffold improves functional recovery after completely transected spinal cord injury in canine, Sci. China Life Sci. 61 (1) (2018) 2–13.

[48] C.D. Pritchard, J.R. Slotkin, D. Yu, H.N. Dai, M.S. Lawrence, R.T. Bronson, F. M. Reynolds, Y.D. Teng, E.J. Woodard, R.S. Langer, Establishing a model spinal cord injury in the African green monkey for the proclinical evaluation of biodegradable polymer scaffolds seeded with human neural stem cells, J. Neurosci. Methods 188 (2) (2010) 258–269.

[49] J.C. Ye, M.J. Ma, Z.Y. Xie, P. Wang, Y. Tang, L. Huang, K. Chen, L.B. Gao, Y.F. Wu, H.Y. Shen, Y.S. Zeng, Evaluation of the neural function of nonhuman primates with spinal cord injury using an evoked potential-based scoring system, Sci. Rep. 6 (2016), 33243.

[50] K. Su, S. Liu, T. Wu, Y.C. Yin, R.P. Zhang, S.L. Li, Y.Z. Zhang, Posterior column acetabular fracture fixation using a W-shaped angular plate: a biomechanical analysis, PLoS One 12 (11) (2017), e0187886.

[51] P. Philippidou, J.S. Dasen, Hox genes: choreographers in neural development, architects of circuit organization, Neuron 80 (1) (2013) 12–34.

[52] Y.M. Yang, R.G. Chen, X.M. Wu, Y.N. Zhao, Y.H. Fan, Z.F. Xiao, J. Han, L. Sun, X. Q. Wang, J.W. Dai, Rapid and efficient conversion of human fibroblasts into functional neurons by small molecules, Stem Cell Rep. 13 (5) (2019) 862–876.

[53] H. Kumamaru, P. Lu, E.S. Rosenzweig, K. Kadoya, M.H. Tuszynski, Regenerating corticospinal axons innervate phenotypically appropriate neurons within neural stem cell grafts, Cell Rep. 26 (9) (2019) 2329–2339, e4.

[54] J. Li, G. Lepski, Cell transplantation for spinal cord injury: a systematic review, BioMed Res. Int. 2013 (2013), 786475.

[55] J.K. Lee, B.H. Zheng, Role of myelin-associated inhibitors in axonal repair after spinal cord injury, Exp. Neurol. 235 (1) (2012) 33–42.

[56] M.S.Y. Yeung, M. Djelloul, E. Steiner, S. Bernard, M. Salehpour, G. Possnert, L. Brundin, J. Frisén, Dynamics of oligodendrocyte generation in multiplesclerosis, Nature 566 (7745) (2019) 538–542.

[57] V. Koprivica, K.S. Cho, J.B. Park, G. Yiu, J. Atwal, B. Gore, J.A. Kim, E. Lin, M. T. Lavigne, D.F. Chen, Z.G. He, EGFR activation mediates inhibition of axon regeneration by myelin and chondroitin sulfate proteogycans, Science 310 (5745) (2005) 106–110.

[58] M. Berry, Z. Ahmed, M.R. Douglas, A. Logan, Epidermal growth factor receptor antagonists and CNS axon regeneration: mechanisms and controversies, Brain Res. Bull. 84 (4–5) (2011) 289–299.

[59] J.L. Lin, Z.C. Xiong, J.H. Gu, Z.R. Sun, S. Jiang, D.W. Fan, W.S. Li, Sirtuins: potential therapeutic targets for defense against oxidative stress in spinal cord injury, Oxid. Med. Cell. Longev. 2021 (2021), 7207692.

[60] P. Lu, L.L. Jones, E.Y. Snyder, M.H. Tuszynski, Neural stem cells constitutively secrete neurotrophic factors and promote extensive host axonal growth after spinal cord injury, Exp. Neurol. 181 (2) (2003) 115–129.

[61] F.F. Liu, A.G. Xuan, Y. Chen, J.D. Zhang, L.P. Xu, Q.J. Yan, D.H. Long, Combined effect of nerve growth factor and brain-derived neurotrophic factor on neuronal differentiation of neural stem cells and the potential molecular mechanisms, Mol. Med. Rep. 10 (4) (2014) 1739–1745.

[62] X. Yi, G.H. Jin, M.L. Tian, W.F. Mao, J.B. Qin, Porous chitosan scaffold and ngf promote neuronal differentiation of neural stem cells in vitro, Neuroendocrinol. Lett. 32 (5) (2011) 705–710.

[63] Z. Han, C.P. Wang, N. Cong, Y.Y. Gu, R. Ma, F.L. Chi, Therapeutic value of nerve growth factor in promoting neural stem cell survival and differentiation and protecting against neuronal hearing loss, Mol. Cell. Biochem. 428 (1–2) (2017) 149–159.

[64] J. Soltys, C. Perrone, J. Knight, Y.M. Draayer, PDFG-AA and BDNF promote neural stem cell differentiation, J. Neurol. Neurophysiol. s4 (2011).

[65] Y. Jiao, B. Palmgren, E. Novozhilova, U.E. Johansson, A.L.S. Engemann, A. Kale, S. I. Stupp, P. Olivius, BDNF increases survival and neuronal differentiation of human neural precursor cells cotransplanted with a nanofiber gel to the auditory nerve in a rat model of neuronal damage, BioMed Res. Int. 2014 (2014), 356415.

[66] K. Yang, H.J. Park, S. Han, J. Lee, E. Ko, J. Kim, J.S. Lee, J.H. Yu, K.Y. Song, E. Cheong, S.R. Cho, S. Chung, S.W. Cho, Recapitulation of in vivo-like paracrine signals of human mesenchymal stem cells for functional neuronal differentiation of human neural stem cells in a 3D microfluidic system, Biomaterials 63 (2015) 177–188.

[67] A. Bakshi, S. Shimizu, C.A. Keck, S. Cho, D.G. LeBold, D. Morales, E. Arenas, E. Y. Snyder, D.J. Watson, T.K. Mclntosh, Neural progenitor cells engineered to secrete GDNF show enhanced survival, neuronal differentiation and improve cognitive function following traumatic brain injury, Eur. J. Neurosci. 23 (8) (2006) 2119–2134.

[68] A. Bonafina, P.A. Fontanet, G. Paratcha, F. Ledda, GDNF/GFRα1 complex abrogates self-renewing activity of cortical neural precursors inducing their differentiation, Stem Cell Rep. 10 (3) (2018) 1000–1015.

[69] N. Sharma, C.D. Deppmann, A.W. Harrington, C. St Hillaire, Z.Y. Chen, F.S. Lee, D. D. Ginty, Long-distance control of synapse assembly by target-derived NGF, Neuron 67 (3) (2010) 422–434.

[70] C.S. Wang, E.T. Kavalali, L.M. Monteggia, BDNF signaling in context: from synaptic regulation to psychiatric disorders, Cell 185 (1) (2022) 62–76.

[71] F. Ledda, G. Paratcha, T. Sandoval-Guzmán, C.F. Ibáñez, GDNF and GFRα1 promote formation of neuronal synapses by ligand-induced cell adhesion, Nat. Neurosci. 10 (2007) 293–300.